NASA Technical Memorandum 81330


NASA-TM-81330 19820002137

# A New Solution-Adaptive Grid Generation Method for Transonic Airfoil Flow Calculations

S. Nakamura and T. L. Holst

October 1981



National Aeronautics and
Space Administration

NASA Technical Memorandum 81330

# A New Solution-Adaptive Grid Generation Method for Transonic Airfoil Flow Calculations

S. Nakamura, Ohio State University, Columbus, Ohio
T. L. Holst, Ames Research Center, Moffett Field, California

NASA
National Aeronautics and
Space Administration

**Ames Research Center**
Moffett Field. California 94035

# A NEW SOLUTION-ADAPTIVE GRID GENERATION METHOD FOR TRANSONIC AIRFOIL FLOW CALCULATIONS

S. Nakamura*
Mechanical Engineering Department
The Ohio State University
206 W 18th Ave
Columbus, Ohio 43210

and

T. L. Holst
NASA Ames Research Center
Moffett Field, California 94035

## 1. INTRODUCTION

Solving airfoil flow problems numerically with minimal number of grid points, or maximizing the accuracy of flow solutions with a fixed number of grid points, has become very important since more practical numerical solutions to three-dimensional airfoil flow problems are being explored. For the purpose of increasing accuracy of flow solutions, grid clustering techniques have been proposed [1,2]. These techniques were used until recently without simultaneous or iterative interaction with the flow solution, but rather the user arbitrarily guessed where fine grids might be needed and then decided how to cluster grid lines.

As an advanced way of clustering grids, the solution-adaptive grid concept was lately proposed [3,4] and shown to be effective in increasing the accuracy of numerical solution to the transonic full potential equation for airfoil flow problems. In the approach of Holst and Brown [4], the grid distribution along an airfoil was adapted to the initial flow solution. Then, grid systems in the flow field were obtained by the elliptic-type grid generation equations devised by Steger and Sorenson [2]. One drawback with this approach is that, while clustering grids along the airfoil is easy, maintaining the same degree of clustering inside the flow field is not. This is because the Steger-Sorenson iterative scheme becomes very slow to converge or even unstable when strong clustering is extended to an area far from the airfoil.

This report decribes a new method of adaptive grid generation for the transonic full potential equation. The present approach requires four steps of computation:

Step 1: Generation of initial grids
Step 2: Solution of full potential equation on the initial grids
Step 3: Generation of solution-adaptive grids
Step 4: Solution of full potential equation on the adaptive grids

*Supported under NASA-Ames University Consortium Joint Research Interchange NCA2-OR565-901.

The solution-adaptive grid generation method proposed in this report has some similarity to the Holst-Brown method when grids are adapted along the airfoil surface, but it determines grids inside the flow field systematically without solving the elliptic grid generation equation. The present approach not only saves computing time but has an advantage that strong clustering along the airfoil surface as well as inside the flow field is very easy.

Although the present method is applicable to clustering grids in the $\xi$-direction (tangent to airfoil surface) as well as in the $\eta$-direction (normal to airfoil surface), we forcus our attention in this report only to that in the $\xi$-direction.

## 2. TRANSONIC FULL POTENTIAL EQUATION

The full potential equation for air flow around an airfoil is given by

$$(\rho\phi_x)_x + (\rho\phi_y)_y = 0 \tag{2.1}$$

$$\rho = [\, 1 - (\, \phi_x^{\,2} + \phi_y^{\,2}\,)(\gamma-1)/(\gamma+1)\,]^{1/(\gamma-1)} \tag{2.2}$$

where $\rho$ is the density nondimensionalized with stagnation density; $\phi_x = u$ and $\phi_y = v$ are velocity components, which are nondimensionalized by the critical sound speed; $\gamma$ is the specific heat ratio of air; x and y are Cartesian coordinates.

The boundary condition for $\phi$ along the airfoil surface is given by $\partial\phi/\partial n = 0$ where $\partial/\partial n$ is the derivative normal to the surface.

In order to apply efficiently the iterative numerical solution techniques such as SOR (successive-over-relaxation) or ADI (alternating-direction-implicit) to solving elliptic partial differential equations, Eq.(2.1) is transformed from the physical domain (x,y) to a computational domain ($\xi$,$\eta$), so the grid lines on the computational domain are rectangular and uniformly spaced in both directions.

The full potential equation on the computational domain is

$$(\rho U/J)_\xi + (\rho V/J)_\eta = 0 \tag{2.3}$$

where

$$U = A_1\phi_\xi + A_2\phi_\eta$$

$$V = A_2\phi_\xi + A_3\phi_\eta$$

$$A_1 = \xi_x^{\,2} + \xi_y^{\,2}\,, \quad A_2 = \xi_x\eta_x + \xi_y\eta_y\,, \quad A_3 = \eta_x^{\,2} + \eta_y^{\,2}$$

$$J = \xi_x\eta_y - \xi_y\eta_x$$

$$\rho = [1-(U\phi_\xi + V\phi_\eta)(\gamma-1)/(\gamma+1)]^{1/(\gamma-1)}$$

Finite difference equations for Eq.(2.3) are written and solved iteratively by using the AF2 iteration scheme detailed in reference [5]. The TAIR (Transonic Airfoil analysis) computer code is used for this purpose.

## 3. GENERATION OF INITIAL GRIDS

Grid generation in Step 1 (initial grids) is performed by solving the elliptic equations originally proposed by Thompson and et al. [1], and revised later by Steger and Sorenson [2]. The alternating-direction-implicit method has been successfully applied here to solving elliptic grid generation equations with grid spacing control. The initial grids may be generated by the hyperbolic grid generation equations [6], but this approach is left open for further study.

### 3.1 Elliptic Grid Generation Equation and Iterative Scheme

The grid generation equation with spacing control may be written in the form

$$\begin{aligned} Ax_{\xi\xi} + Bx_{\xi\eta} + Cx_{\eta\eta} + Ex_{\xi} + Fx_{\eta} &= 0 \\ Ay_{\xi\xi} + By_{\xi\eta} + Cy_{\eta\eta} + Ey_{\xi} + Fy_{\eta} &= 0 \end{aligned} \tag{3.1}$$

where

$$A = x_{\eta}^{2} + y_{\eta}^{2}$$

$$B = -2(x_{\xi}x_{\eta} + y_{\xi}y_{\eta})$$

$$C = x_{\xi}^{2} + y_{\xi}^{2}$$

$$E = J^{2}\exp[-c_{n}(\eta_{max}-\eta)]P_{1}(\xi) \tag{3.2a}$$

$$F = J^{2}\exp[-c_{n}(\eta_{max}-\eta)]Q_{1}(\xi) \tag{3.2b}$$

$$J = x_{\xi}y_{\eta} - x_{\eta}y_{\xi}$$

In the above equations, $c_n$ is a user-specified constant; $P_1(\xi)$ and $Q_1(\xi)$ are given by

$$P_{1}(\xi) = J^{-1}(y_{\xi}R_{1} - y_{\eta}R_{2})|_{\eta=\eta_{max}}$$

$$Q_{1}(\xi) = J^{-1}(-y_{\xi}R_{1} + x_{\xi}R_{2})|_{\eta=\eta_{max}}$$

where

$$R_{1} = -J^{-2}(Ax_{\xi\xi} - 2Bx_{\xi\eta} + Cx_{\eta\eta})|_{\eta=\eta_{max}}$$

$$R_{2} = -J^{-2}(Ay_{\xi\xi} - 2By_{\xi\eta} + Cy_{\eta\eta})|_{\eta=\eta_{max}}$$

The difference form of Eq.(3.1) may be written as

$$Lx = (A\delta_{\xi\xi} + B\delta_{\xi\eta} + C\delta_{\eta\eta} + E\delta_{\xi} + F\delta_{\eta})x = 0$$
$$Ly = (A\delta_{\xi\xi} + B\delta_{\xi\eta} + C\delta_{\eta\eta} + E\delta_{\xi} + F\delta_{\eta})y = 0 \qquad (3.3)$$

where $\delta_{ff}$ and $\delta_{f}$ are second order and first order difference operators, respectively. L in the above equations represents the entire difference operator after the first equality sign.

## 3.2 Iterative Scheme

The alternating-direction-implicit (ADI) iterative scheme using residuals may be written as

$$Mv = -\omega Lx^{(t-1)} \qquad (3.4a)$$

$$Mw = -\omega Ly^{(t-1)} \qquad (3.4b)$$

where

$$v = x^{(t)} - x^{(t-1)}$$

$$w = y^{(t)} - y^{(t-1)}$$

and where t is the iteration number, $\omega$ is a relaxation parameter and M is an iterative operator that is chosen to be similar to L. As M becomes closer to L, the iterative scheme becomes more implicit, so the convergence rate increases. Here, we choose M as

$$M = (\alpha + C\delta_{\eta\eta} + F\delta_{\eta})(\alpha + A\delta_{\xi\xi} + E\delta_{\xi})/\alpha \qquad (3.5)$$

where $\alpha$ is an acceleration parameter varied at each iteration. Since difference operators in $\xi$ and $\eta$ are separated, each of Eq.(3.4) can be solved in two steps:

$$z = \alpha\,(\alpha + A\delta_{\xi\xi} + E\delta_{\xi})^{-1}\,\mathrm{RHS}$$
$$v \text{ or } w = (\alpha + C\delta_{\eta\eta} + F\delta_{\eta})^{-1}z \qquad (3.6)$$

where RHS represents the right side of Eq.(3.4a) or Eq.(3.4b). In order to increase stability of iteration, either forward differencing or backward differencing, whichever increases the diagonal terms of the tridiagonal matrices, is selected for $\delta_{\xi}$ and $\delta_{\eta}$ at each grid.

The values of $P_1(\xi)$ and $Q_1(\xi)$ are recalculated after each iteration by using the most updated values of x and y. However, large changes of $P_1$ and $Q_1$ in any two consecutive iterations cause instability in the iterative scheme of mesh generation. In order to prevent such large changes, using underrelaxation for $P_1$ and $Q_1$ is necessary.

## 4. ADAPTIVE GRID RELOCATION METHOD

### 4.1 Algorithm

Assume that an initial grid system is given, on which the initial solution of the full potential equation is obtained. The word 'adaptive' indicates that a new improved grid system is generated adapting to the initial solution. The new grid system is obtained by relocating the initial grids along each $\xi$ line without changing the shape of the $\xi$ lines.

Let us pay attention to the grids on the airfoil surface (a $\xi$ line). Denote $s=s(\xi)$ as the circumference on the $\xi$ line between $\xi$ and $\xi=1$ (reference point) on the initial grid system (see Fig.1). The circumference between grid i and i=1 (reference grid) may be denoted as $s_i=s(\xi_i)$. Now, we move grid i to a new location on the same $\xi$ line at circumference $s_i'=s(\xi_i')$, where $\xi_i'$ is the value of $\xi$ for the i-th grid after moving on the initial computational domain. Relocation of all the grids except the reference grid is achieved if one-to-one correspondence between $\xi$ and $\xi'$ is specified by a functional relation as

$$\xi = T(\xi') \quad \text{or equivalently} \quad \xi'=T^{-1}(\xi) \tag{4.1}$$

In the above equation, $T(\xi')$ is a monotonic function of $\xi'$, given by

$$T(\xi') = A[\xi'- 1 + \int_1^{\xi'} \psi(\xi'')d\xi''] + 1 \tag{4.2}$$

where $\psi$ is the grid density function described in the next paragraph, and A is a normalization constant determined by the condition,

$$T(\xi_{max}') = \xi_{max} = \xi_{max}'$$

The grid density function $\psi$ is determined by solving

$$- d^2\psi(\xi')/d\xi'^2 + \sigma\psi(\xi') = f|\partial\rho/\partial\xi'| + g|k| \tag{4.4}$$

In the above equation, $\sigma$ is a parameter to adjust the propagation of the effect of grid spacing control along the $\xi$ line: f is the parameter that emphasizes the effect of the fluid density gradient: k is the curvature of the airfoil surface and g is to control the effect of the airfoil surface curvature on grid density.

In principle, the above algorithm may be applied to each $\xi$ line independently. However, we determine $T(\xi')$ using $\rho(\xi',\eta)$ along the airfoil surface first, and then use the same $T(\xi')$ for all the $\xi$ lines. The values of $\xi_i'$ for new grids along the j-th $\eta$ line may be denoted by $\xi_{i,j}'$. Since grids are relocated along the initial $\eta$ lines, the values of x and y for the new grids are found from the relations,

$$x_{i,j}' = x(\xi_{i,j}',\eta_j)$$

$$y_{i,j}' = y(\xi_{i,j}',\eta_j)$$

by using interpolations, where $x=x(\xi,\eta)$ and $y=y(\xi,\eta)$ are the transformation between the physical domain and the initial computational domain. Interpolations are necessary because $x(\xi,\eta)$ and $y(\xi,\eta)$ are known only on the initial grids, $(\xi_i,\eta_j)$.

### 4.2 Schematic Illustration

In order to explain the grid relocation algorithm procedure more qualitatively, suppose in Eq.(4.4) $g=0$ and $\partial\rho/\partial\xi'$ behaves as a delta function at $\xi_o$, for illustration purpose, as shown in Fig.2-A. The solution of Eq.(4.4) with a set of specified $\sigma$ and f is illustrated by a solid line in Fig. 2-B.

By introducing $\psi$ thus determined into Eq.(4.2), $T(\xi')$ with A=1 becomes Curve-a' in Fig. 2-C. After normalization, $T(\xi')$ becomes Curve-a in the same figure. Curves-b and c are obtained by changing $\sigma$ and f as follows:

Curve-b : only f is decreased
Curve-c : $\sigma$ and f are both increased

With a decrease in f, $\psi$ will become smaller by a factor. The curve-b of $T(\xi')$ in Fig. 2-C becomes closer to a straight line which is the case when $f=g=0$. With a simultaneous increase in both $\sigma$ and f, the distribution of $\psi$ becomes more sharply peaked about $\xi_o$. Consequently, a very sharp increase in $T(\xi')$ occurs around $\xi_o$ as illustrated by Curve-c in Fig. 2-C.

Although the qualitative effect of altering $\sigma$ and f are explained by considering a delta-function-like distribution in $\partial\rho/\partial\xi'$, the distribution of $\partial\rho/\partial\xi'$ in actual problems is a continuous function with a large change across a shock.

## 5. NUMERICAL STUDY

The effect of applying the proposed adaptive grid generation is investigated by considering a lifting flow of the NACA 0012 airfoil with the following parameters:

| | |
|---|---|
| Attack angle | $2^o$degree |
| $M_{inf}$ | 0.75 |
| Number of grid points | 99x25(coarse grid) |

The grid systems with 99x25 grid points with or without solution adapting will be referred to as 'coarse grid'.

As the reference flow solution to which the present numerical results are to be compared, the same flow problem was run on a fine grid system (245 grids in the $\xi$-direction and 56 grids in the $\eta$-direction). The pressure coefficient distribution for the reference calculation is

plotted with a plain black line in every figure for the pressure coefficient distribution calculated with the coarse grids. The lift, drag and moment coefficients calculated with the reference fine grid system are CL = 0.5997, CD = 0.0190, CM = -0.0268, respectively.

Figure 3 shows the initial grids generated in Step 1 and the CP (pressure coefficient) distribution obtained from Step 2. In Fig. 3-A, only the inner 14 $\xi$ lines are shown for brevity and a better resolution of grid points along the airfoil surface. The line with diamonds in Fig. 3-B is the result of the present calculation. The diamonds show the location of grids. The graph is stretched toward both leading and trailing edges. The large disagreement in the pressure coefficient distribution at the shock from the reference CP distribution is typical when grids are coarse across a shock.

Figure 4-A is the result of adaptive grids generated in Step 3 with f=10, $\sigma$=0.5. Denser grids at the leading edge are caused by large values of $\partial\rho/\partial\xi$ at the leading edge. A strong clustering occurs also at the shock. In Fig. 4-B, the pressure coefficient distribution obtained using the adaptive grids in Fig. 4-A is compared with the reference pressure coefficient. The agreement in the CP distribution at the shock is excellent.

Figure 5-A shows the same results as Fig. 4 except with f=10 and $\sigma$=0.1. Clustering at the leading edge and at the shock is stronger than in Fig. 4-A. Figure 5-B shows that the agreement of CP distribution at the shock is good. However, the disagreement in CP inside the supersonic bubble, and after the shock, is larger than in Fig. 4-B. The reason is attributed to coaser grids in the $\xi$-direction in other areas than the leading edge and the shock.

Figure 6 shows the same results as Fig. 4 except with f=10 and $\sigma$=1.5. With a larger value of $\sigma$, the effects of clustering grids become more localized. However, when $\sigma$ only is increased with f unchanged as in this case, the overall clustering effect becomes weaker. This is the reason why the results of Figs. 6-A and 6-B both fall in between those of Fig. 3 and Fig. 4.

In Fig. 7, clustering at the leading edge is supressed so grid lines only around the shock are strongly clustered. Agreement in the shock with the reference case is excellent. The change of CP across the shock is even sharper than the reference CP distribution.

Figure 8-A shows the adaptive grid system in which the number of grids along the upper airfoil surface is artificially increased while that in the lower surface is drastically decreased. This increase of grids above airfoil is done by artificially changing the value of $\partial\rho/\partial\xi$ in Eq.(4.4). In spite of finer grids in the supersonic region than the previous cases, agreement in the CP distribution, particularly across the shock, is worse. However, the shape of the CP distribution in the supersonic bubble is more similar to the reference case than any other case. The agreement in the shape is due to the fine grids in the $\xi$-direction, but disagreement in values is attributed to coarseness of grids in the $\eta$-direction. This observation suggests importance of

improving grid configuration in the leading edge region or importance of improving the accuracy of the difference equation in the same area. The disagreement of the calculated CP distribution from the reference distribution in the trailing edge area is due to coarse grids. This trailing edge coarseness could also cause a small error in the circulation and therefore be partly responsible for the error in the shock position.

The difference equations used for the supersonic region are essentially the first-order-accuate upwind difference scheme. In order to maintain the upwind difference scheme, TAIR had assumed that the flow in the supersonic region is in the positive direction of $\xi$ if $\xi>\xi_{half}$ or in the negative direction of $\xi$ if $\xi<\xi_{half}$, where $\xi_{half}=\xi_{max}/2$. Until adaptive grids were applied, this algorithm did not cause any problem, because $\xi_{half}$ was located in the vicinity of the leading edge any way, and maintained enough distance from the boundary of supersonic regions. However, when adaptive grids are used, $\xi_{half}$ may move into a supersonic region, particularly when grids are strongly clustered on one side of airfoil where a supersonic region appears. If this happens, the upwind difference scheme is violated and an instability of iteration is resulted. In order to correctly apply the upwind difference scheme, $\xi_{half}$ was redefined as the value of $\xi$ at the leading edge on the adaptive grids. Figure 9 shows the CP distribution calculated by TAIR before redefining $\xi_{half}$ using an adaptive grid system with very strong clustering, where the CP distribution behaves erratically in the supersonic region because the upwind difference scheme was violated.

## 6. CONCLUSIONS

A new efficient method of generating adaptive grids for the transonic full potential equation is presented. With the present method, adapting grids to high curvature surfaces, shocks, and wherever high flow acceleration or deceleration occurs is easy. Since the adapting procedure needs the solution of a one-dimensional boundary value problem only once, the present method consumes a very small fraction of the computational cost required to generate a new grid system by the standard grid generation method. The additional advantage of the present method is that an accurate initial guess for the iterative solution on the new adaptive grid can be easily obtained from the initial flow solution by using the same interpolation procedure as used for grid relocation, so computing time for the flow solution on the adaptive grids can be substantially saved also.

The flow solution on the adaptive grids show that accuracy in the pressure coefficient distribution across the shock is substantially improved with grid clustering. The CP distribution in the supersonic bubble is more sensitive to the grid spacing in the $\xi$-direction than in the subsonic flow region. It is also affected by the grid spacing in the $\eta$-direction particularly in the leading edge area where flow acceleration is extremely high.

While optimal distribution of grids along the airfoil surface is important, better grid clustering in the $\eta$-direction around the leading edge seems to be vital to further improvement of accuracy in the flow solution.

## ACKNOWLEDGEMENT

A part of the computations was performed, using AMDAHL 470 at Instruction and Research Computer Center of The Ohio State University, with the fund provided by the Mechanical Engineering Department of The Ohio State University. The authors are indebted to Mr. Feng-Jee Tsai, who is a Graduate Research Associate at The Ohio State University, for his assistance in running programs and typing this manuscript using the Wylbur language.

## REFERENCES

[1] Thompson, J. F., Thames, F. C., and Mastin, C. M., "Automatic Numerical Generation of Body-Fitted Curvilinear Coordinate System for Field Containing Any Number of Arbitrary Two-Dimensional Bodies," Journal of Computational Physics, Vol. 15, 1974, pp. 299-319.

[2] Steger, J. L. and Sorenson, R. L., "Automatic Clustering Near a Boundary in Grid Generation with Elliptic Partial Differential Equations," Journal of Computational Physics, Vol. 33, No. 3, Dec. 1979, pp.405-410.

[3] Dwyer, H. A., Kee, R. J., and Sanders, B. R.,"Adaptive Grid Method for Problems in Fluid Mechanics and Heat Transfer," AIAA Journal, Vol. 18, No. 10, Oct. 1980, pp. 1205-1212.

[4] Holst, T. L. and Brown, D.,"Transonic Airfoil Calculations Using Solution-Adaptive Grids," AIAA 5th Computational Fluid Dynamics Conference, Palo Alto, California, June 22-23, 1981.

[5] Holst, T. L., "A Fast, Conservative Algorithm for Solving the Transonic Full-Potential Equation," Proceedings of AIAA Fourth Computational Fluid Dynamics Conference, July 1979, pp. 109-121. (See also AIAA Journal, Vol. 18, No. 12, Dec. 1980, pp. 1431-1439.)

[6] Steger, J. L. and Chaussee, D. S., "Generation of Body Fitted Coordinates Using Hyperbolic Partial Differential Equations," FSI Report 80-1, Jan. 1980.

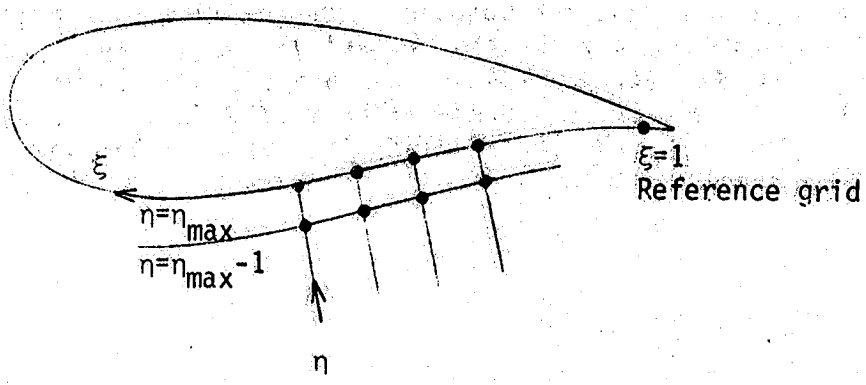


A)

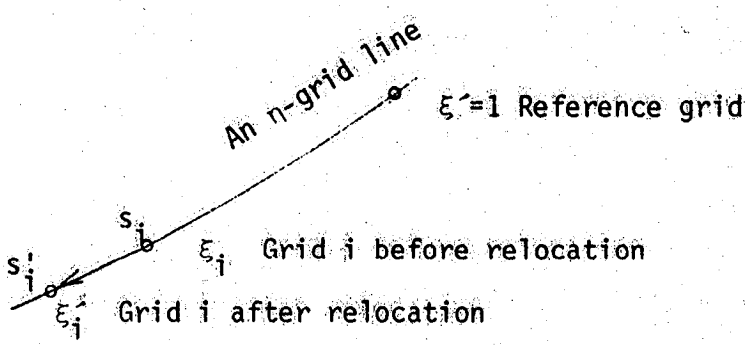


B)

Fig. 1. Schematic of grid point relocation algorithm. A) Detail around the airfoil. B) Detail along an η-grid line.

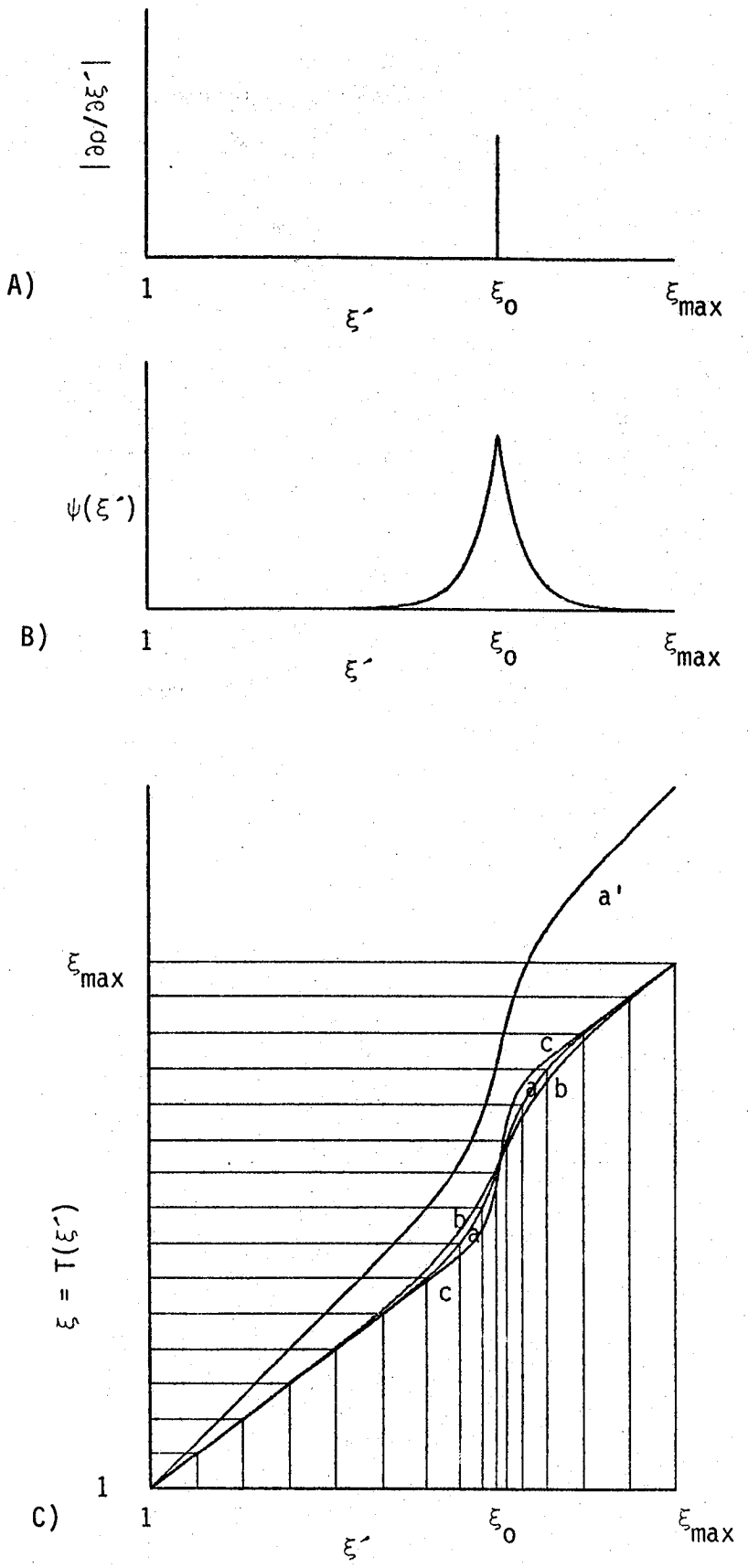


Fig. 2. A simple example using the present grid-point relocation algorithm. A) Density gradient forcing function. B) Resulting grid density function. C) Resulting clustered arc-length distribution on the airfoil surface.

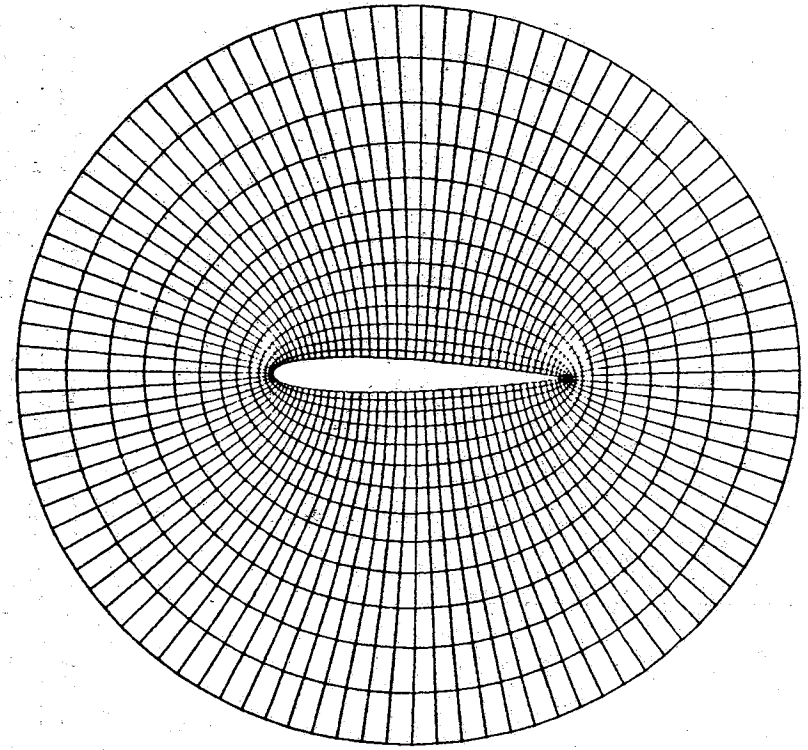

Fig. 3-A Initial Grids
(only 14 inner n-lines are plotted)

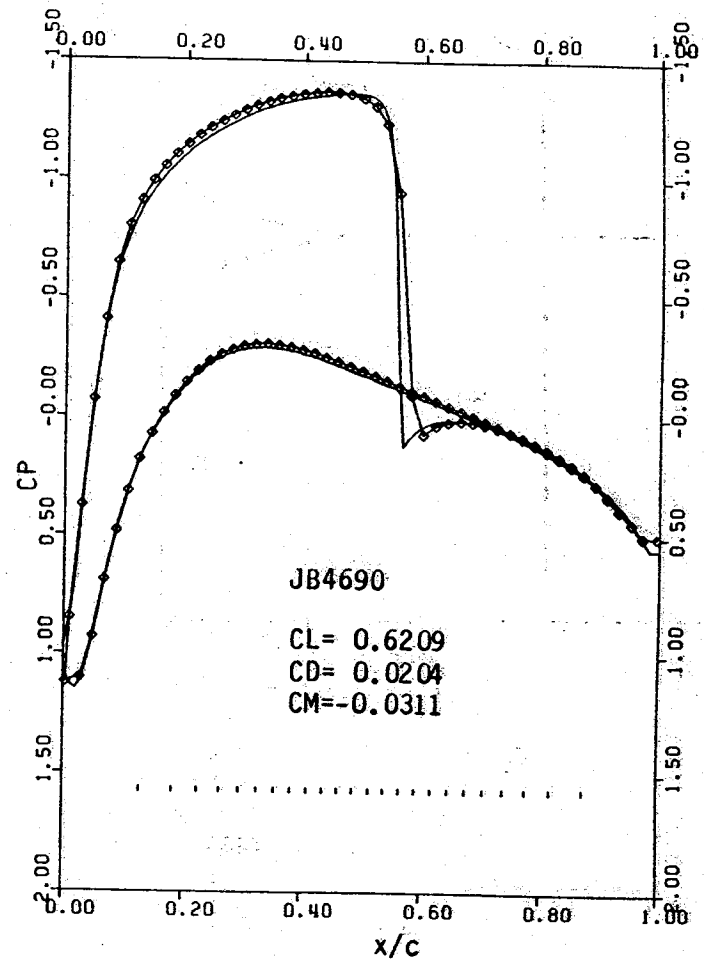


Fig. 3-B CP Distribution
(The graph is stretched toward both leading and trailing edges for better resolution of curves)

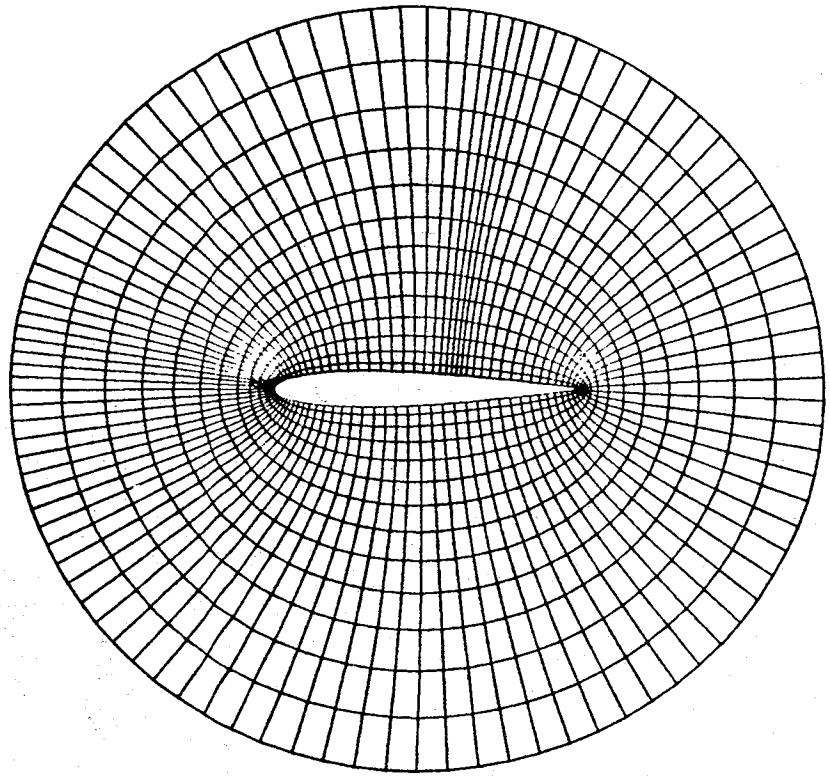

f=10, $\sigma$=0.5

Fig. 4-A Adaptive Grids
(only 14 inner $\eta$-lines are plotted)

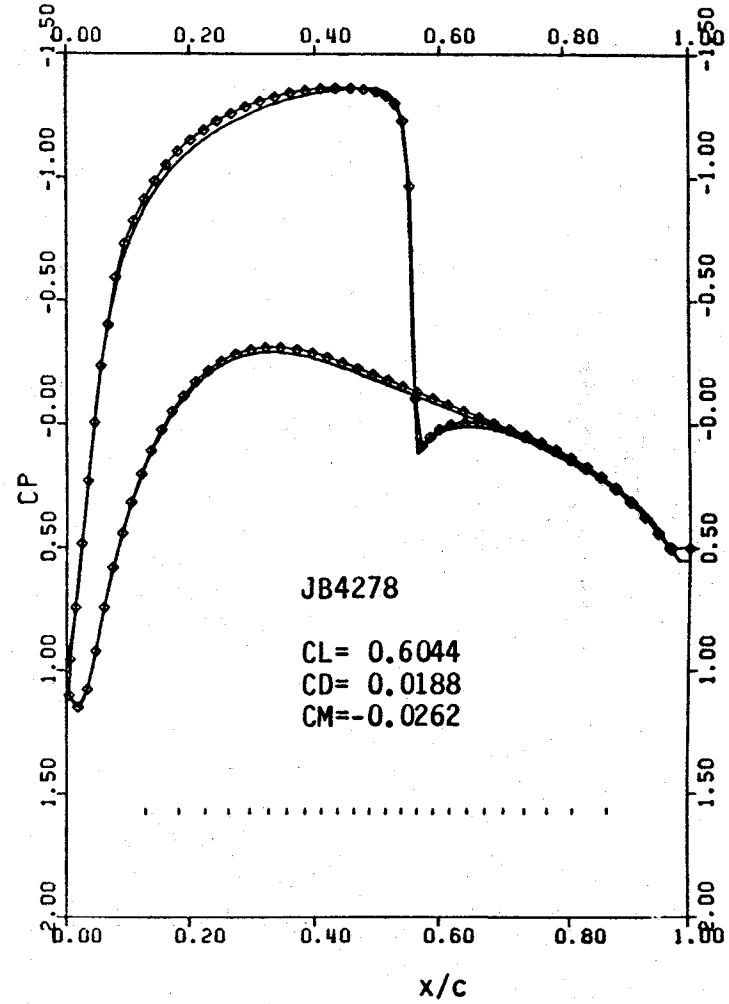


Fig. 4-B CP Distribution
(The graph is stretched toward both leading and trailing edges for better resolution of curves)

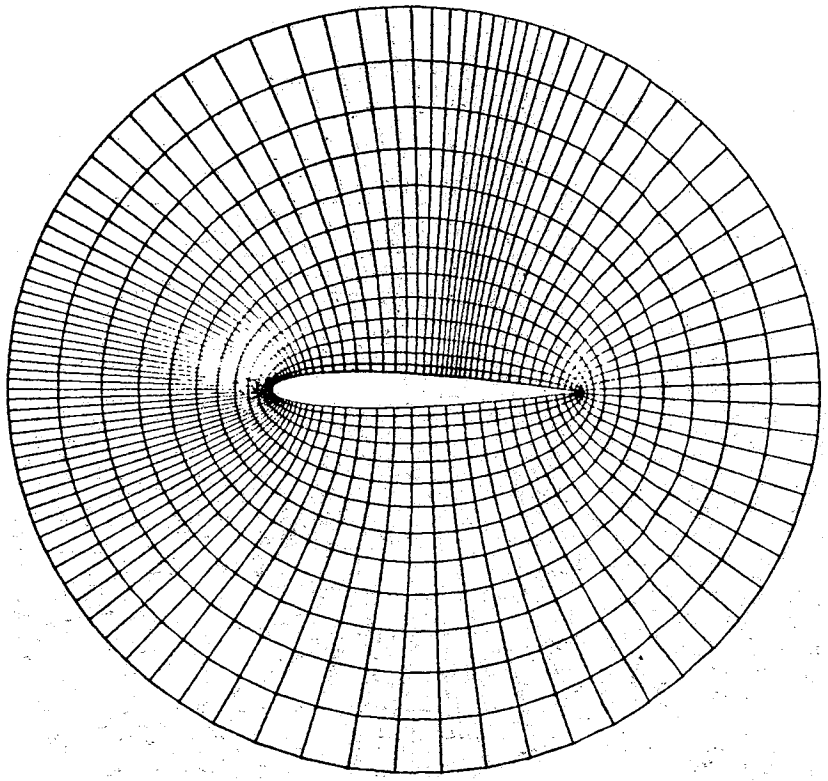

f=10, $\sigma$=0.1

Fig. 5-A Adaptive Grids
(only 14 inner η-lines are plotted)

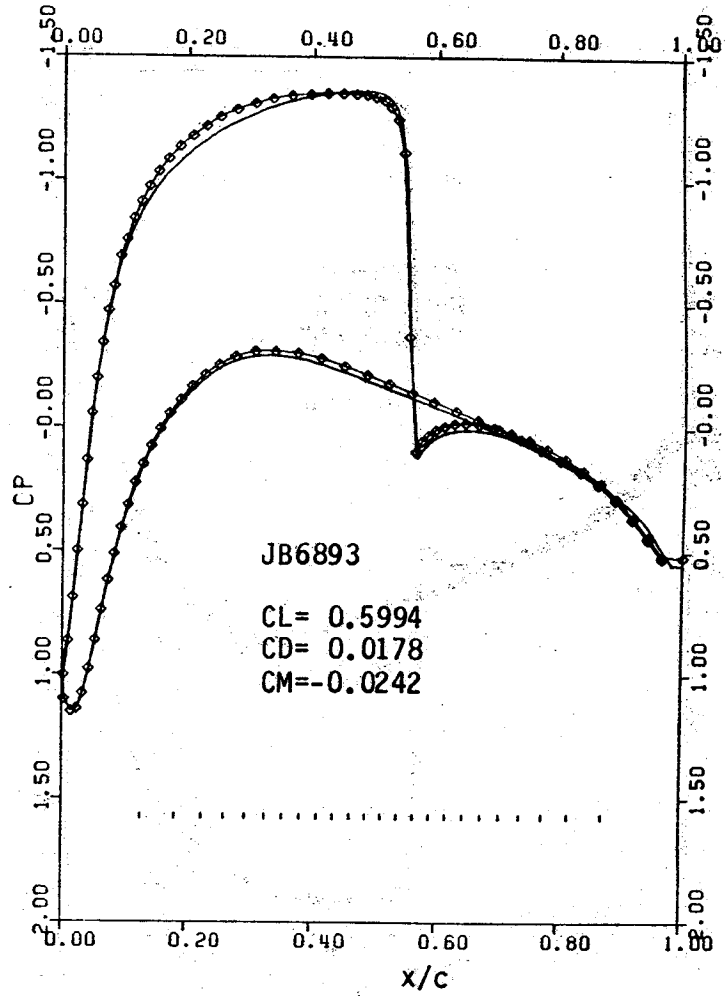


Fig. 5-B CP Distribution
(The graph is stretched toward both leading and trailing edges for better resolution of curves)

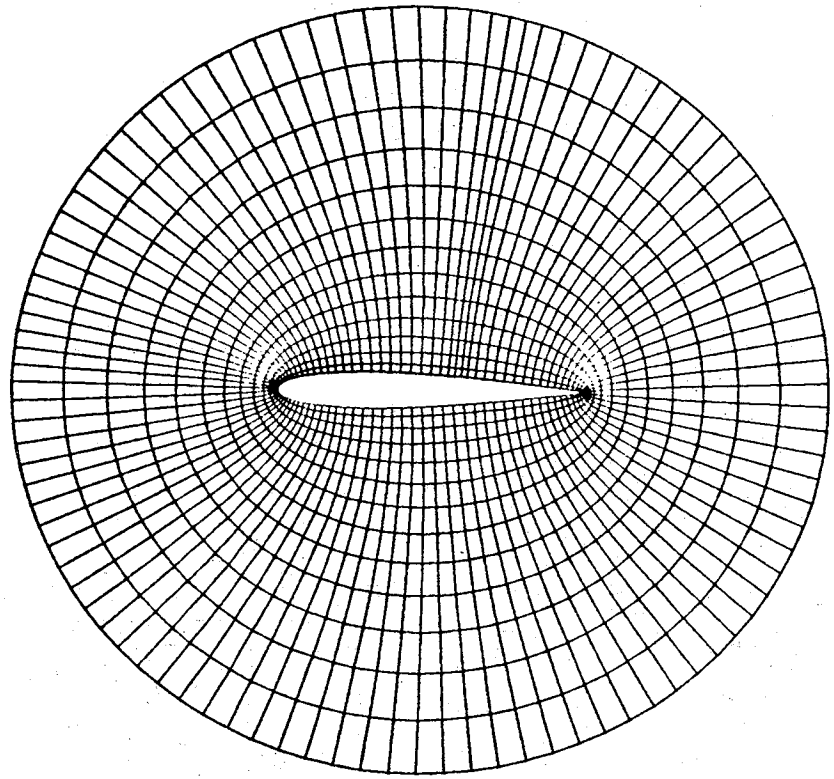

f=10, $\sigma$=1.5

Fig. 6-A Adaptive Grids
(only 14 inner $\eta$-lines are plotted)

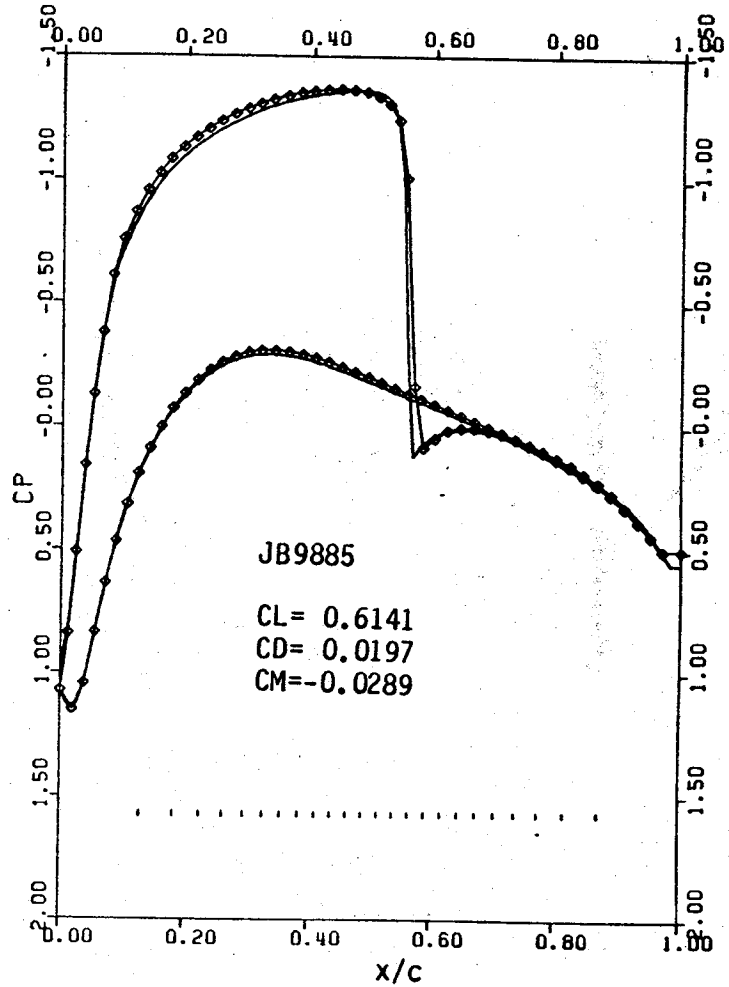


Fig. 6-B CP Distribution
(The graph is stretched toward both leading and trailing edges for better resolution of curves)

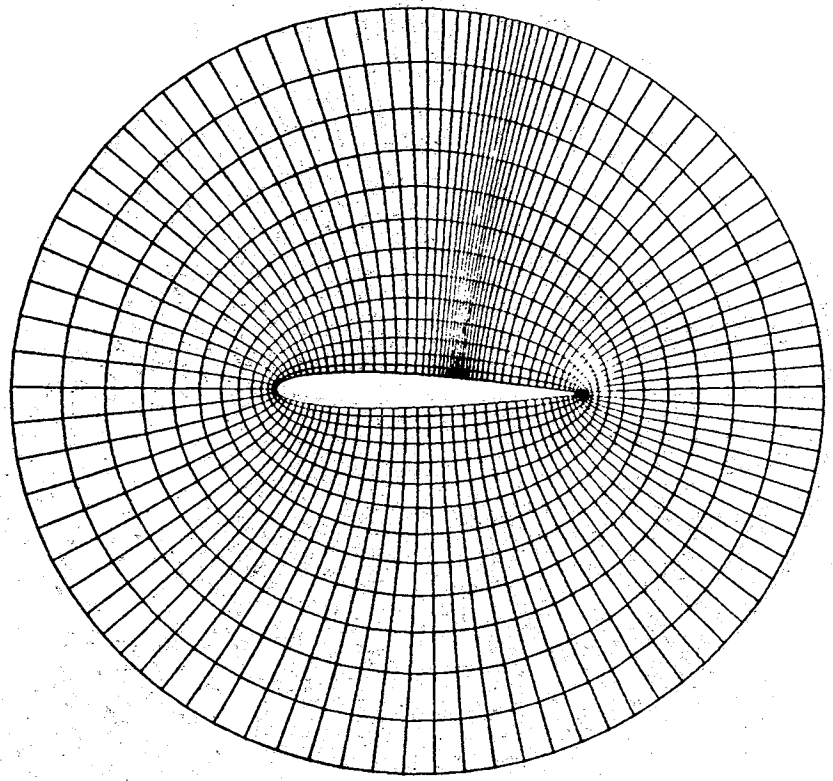

f=20, $\sigma$=0.3
except f=0 for $40<\xi'<60$

Fig. 7-A Adaptive Grids
(only 14 inner $\eta$-lines are plotted)

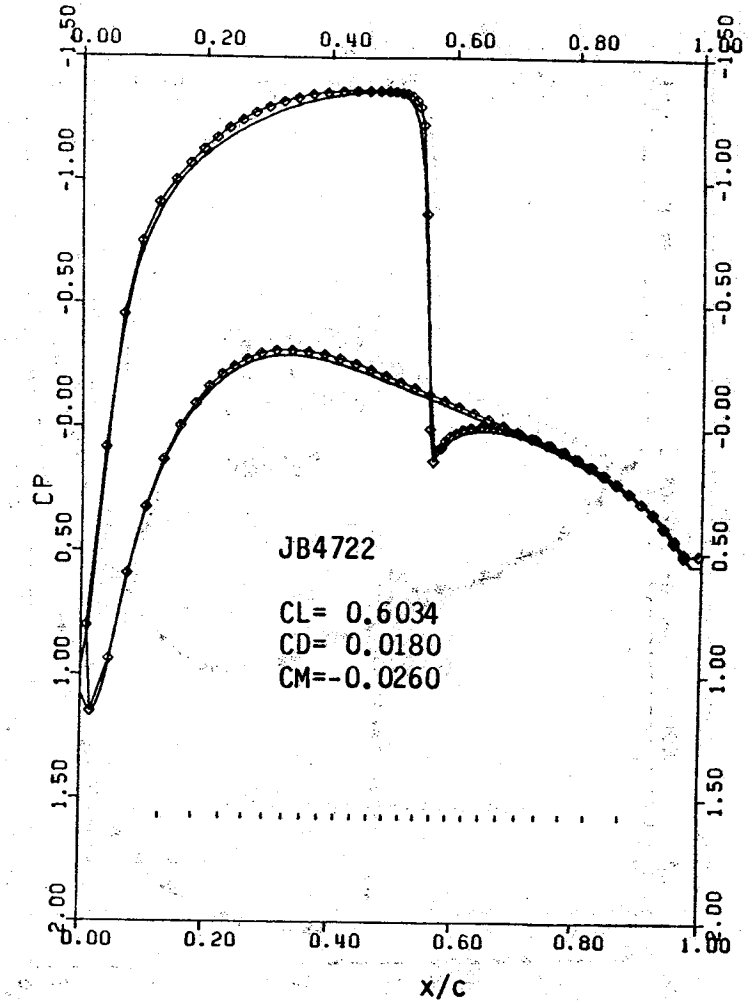


Fig. 7-B CP Distribution
(The graph is stretched toward both leading and trailing edges for better resolution of curves)

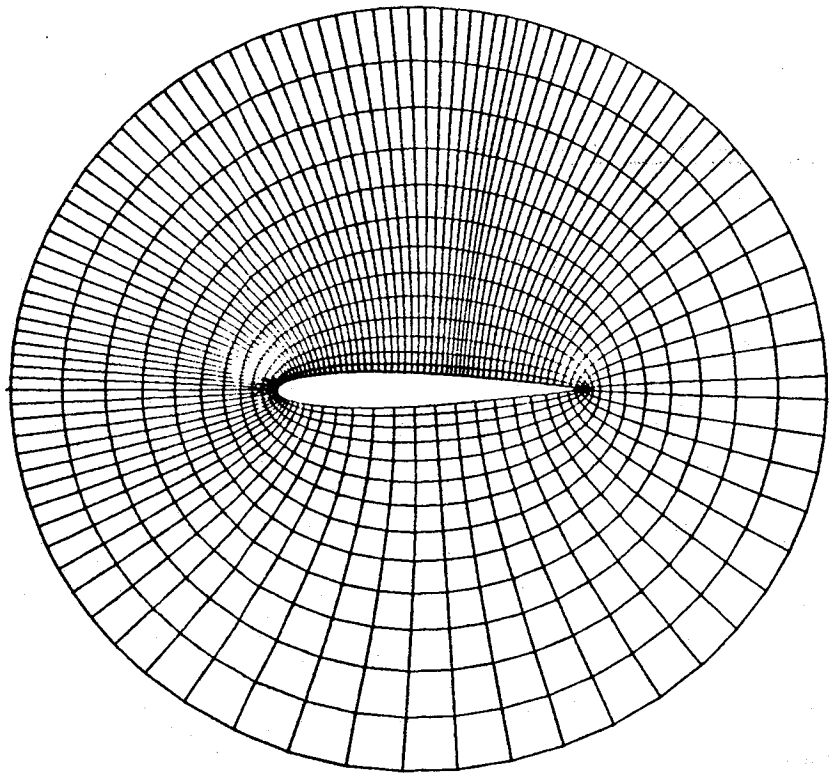

f=20, $\sigma$=0.3
except f=0 for $1<\xi'<40$

Fig. 8-A Adaptive Grids
(only 14 inner $\eta$-lines are plotted)

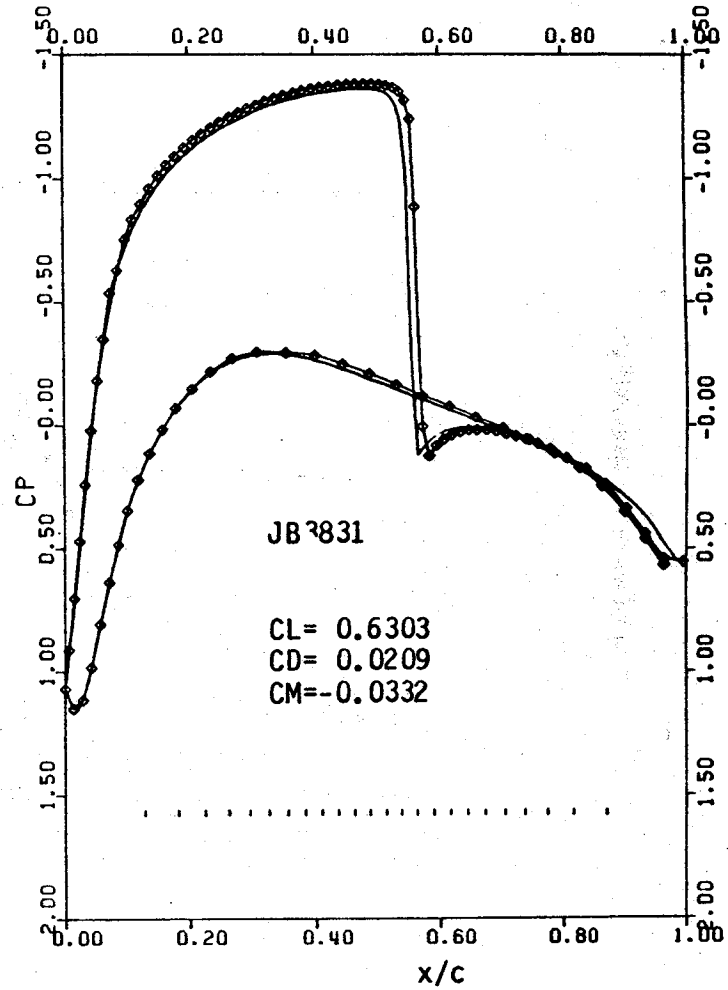


Fig. 8-B CP Distribution
(The graph is stretched toward both leading and trailing edges for better resolution of curves)

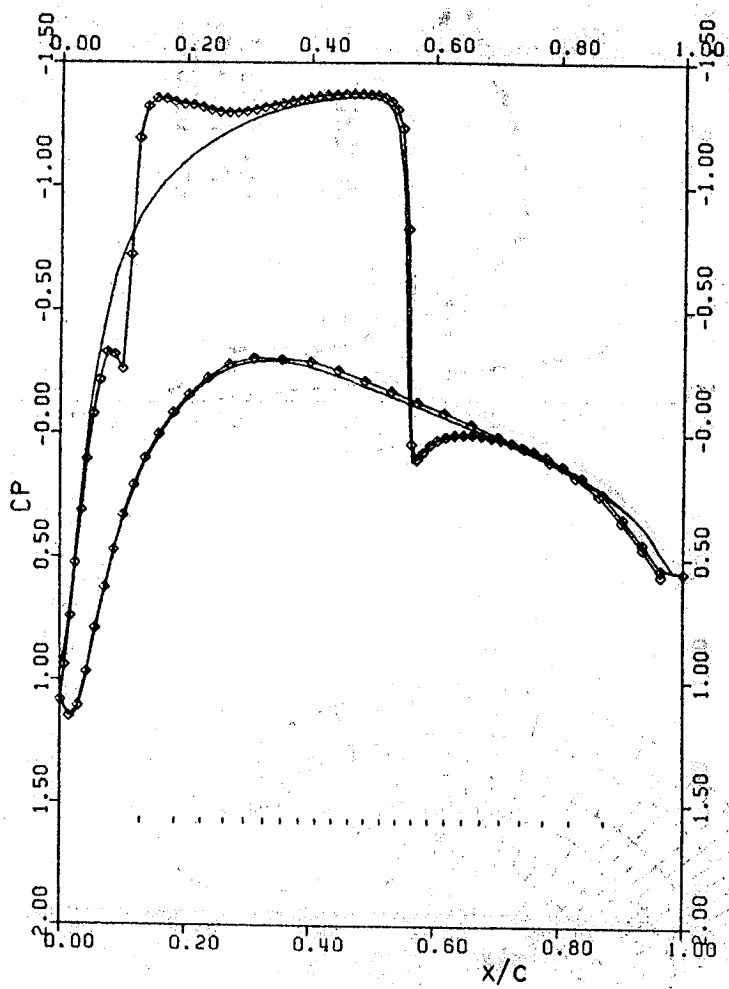


Figure 9 CP distribution Calculated before $\xi_{half}$ was Redefined.

| 1. Report No. | 2. Government Accession No. | 3. Recipient's Catalog No. |
|---|---|---|
| NASA TM-81330 | | |

| 4. Title and Subtitle | 5. Report Date |
|---|---|
| A NEW SOLUTION-ADAPTIVE GRID GENERATION METHOD FOR TRANSONIC AIRFOIL FLOW CALCULATIONS | October 1981 |
| | 6. Performing Organization Code |
| 7. Author(s) | 8. Performing Organization Report No. |
| S. Nakamura* and T. L. Holst | A-8733 |
| | 10. Work Unit No. |
| 9. Performing Organization Name and Address | 505-31-11 |
| Ames Research Center, NASA<br>Moffett Field, Calif. 94035 | 11. Contract or Grant No. |
| | 13. Type of Report and Period Covered |
| 12. Sponsoring Agency Name and Address | Technical Memorandum |
| National Aeronautics and Space Administration<br>Washington, D.C. 20546 | 14. Sponsoring Agency Code |

15. Supplementary Notes

*The Ohio State University
206 W. 18th Ave.
Columbus, Ohio, 43210

16. Abstract

A new algorithm for generating solution-adaptive grids (SAG) about transonic airfoil configurations is presented. The clustering algorithm is controlled by a second-order, ordinary differential equation which uses the airfoil surface density gradient as a forcing function. The solution to this differential equation produces a new surface grid distribution which is automatically clustered in regions with large gradients. The interior grid points are established from this surface distribution by using a new interpolation scheme which is fast and retains the desirable properties of the original grid generated from the standard elliptic equation approach. Numerical results are presented showing significant improvement in accuracy for the SAG grids relative to standard grids using the same number of grid points.

| 17. Key Words (Suggested by Author(s)) | 18. Distribution Statement |
|---|---|
| Grid generation<br>Transonic flow<br>Numerical methods | Unlimited<br><br>STAR Category - 02 |

| 19. Security Classif. (of this report) | 20. Security Classif. (of this page) | 21. No. of Pages | 22. Price* |
|---|---|---|---|
| Unclassified | Unclassified | 20 | $5.00 |

*For sale by the National Technical Information Service, Springfield, Virginia 22161